Physica Scripta

PAPER

Analysis of fusion cross-section and S-factor of $^{13}C + ^{12,13}C$ reactions for different density distributions at astrophysical energies

Murat Aygun[1] **and Gokhan Kocak**[2]

[1] Department of Physics, Bitlis Eren University, 13000, Bitlis, Turkey
[2] Department of Physics, Erciyes University, 38030, Kayseri, Turkey

E-mail: gkocak@erciyes.edu.tr

Keywords: fusion reaction, S-factor, density distribution, optical model, double folding model.

OPEN ACCESS

RECEIVED
14 September 2023

REVISED
25 November 2023

ACCEPTED FOR PUBLICATION
12 December 2023

PUBLISHED
22 December 2023

Abstract

The effect of the various density distributions on $^{13}C + ^{12,13}C$ reactions is investigated by using the optical model at energies near and below Coulomb barrier. For this purpose, five different density distributions of the ^{12}C and ^{13}C nuclei are used to produce the real potential over the double folding model. To make a comprehensive analysis, the fusion cross-sections, S-factor and elastic cross-sections are simultaneously analyzed at astrophysical energies. It is seen that the theoretical results are in good agreement with the experimental data. In this study, the hindrance characteristics of the S-factors for the $^{13}C + ^{12,13}C$ reactions are also examined at low energies, and hindrance behavior is not observed.

1. Introduction

Fusion reactions with carbon isotopes at astrophysical energies have been a subject of intensive study for several decades [1, 2]. For example, carbon fusion is a crucial process in the late evolution of large stars and explosive astronomical events like Type Ia supernovae and x-ray superbursts [3]. Several resonances have been discovered for the $^{12}C + ^{12}C$ fusion reaction nearly 60 years ago. Resonance behavior has been also observed at lower energies in some experiments conducted after this date. Recently, a strong resonance have been reported at $E_{cm} = 2.14$ MeV [4]. For astrophysical scenarios, the most important energy range varies between $E_{cm} = 1 - 3$ MeV. Unfortunately, because of the experimental difficulties, this crucial energy range is only partially measured at energies above $E_{cm} = 2.14$ MeV [5]. Therefore, it is very important to use reliable extrapolation methods for these unmeasurable energy ranges.

Several theoretical methods, such as wave-packet dynamics [6], density-constrained time dependent Hartree–Fock method [7], barrier penetration model by using the Krappe-Nix-Sierk potential [8] and coupled channel calculations [9, 10] have been used to explain unexpected resonance features of fusion reactions with $^{12}C + ^{12}C$ system at energies near and below the Coulomb barrier. These models supports that risind trend of S-factor towards low energies. As an another theoretical model, the hindrance model shows that the $^{12}C + ^{12}C$ system S-factor reaches a maximum value and then declines sharply [11, 12]. Unfortunately, many of these methods are unable to clarify resonance-like structure of the $^{12}C + ^{12}C$ fusion cross-section at astrophysical energies. The complex resonance structure and the lack of experimental data at astrophysical energies hinder the understanding of the $^{12}C + ^{12}C$ reaction. Because of these reasons, the reactions with carbon isotopes like $^{13}C + ^{12}C$ and $^{13}C + ^{13}C$ are very important to understand complex structure of carbon-carbon system [13].

The connection between the structure and reactions in nuclear physics has massive importance because of the reactions conducted by unstable and stable systems. Therefore, the determination of the density distribution of any nucleus is vital in the analysis of different nuclear interactions [14–17]. In this paper, a comprehensive analysis is performed for five different density distributions of the $^{12,13}C$ nuclei by using microscopic nucleon-nucleon double folding model (NN-DFM) together with a weak shallow imaginary potential. The fusion cross-sections, S-factor and elastic cross-sections are examined for the $^{13}C+^{12}C$ and $^{13}C+^{13}C$ systems at astrophysical energies, simultaneously. We also investigate the hindrance characteristics of the $^{13}C + ^{12,13}C$ reactions which is

a topic frequently discussed in the literature [11–13]. Then, we compare the theoretical results with the experimental data and obtain good agreement.

In the next section, we introduce the our theoretical model and the microscopic potentials used in these calculations. Then, we show the results of the $^{13}C+^{12,13}C$ reactions in section 3. Section 4 is devoted to the summary and conclusion.

2. Theoretical framework

In this section, we present the calculation procedures and density distributions which is used in this analysis. In this way, we use the double folding model based on the optical model calculations, and describe the details in the following subsections.

2.1. Optical model

The effective potential ($V_{\text{Effective}}(r)$) of our theoretical analyses consists of

$$V_{\text{Effective}}(r) = V_{\text{Nuclear}}(r) + V_{\text{Coulomb}}(r) + V_{\text{Centrifugal}}(r). \tag{1}$$

Among these potentials, the Coulomb and centrifugal potentials are well known. In this context, the Coulomb potential [18] due to a charge $Z_P e$ interacting with a charge $Z_T e$ distributed uniformly over a sphere of radius R_c is given by

$$V_{Coulomb}(r) = \frac{1}{4\pi\epsilon_\circ}\frac{Z_P Z_T e^2}{r}, \; r \geqslant R_c \tag{2}$$

$$= \frac{1}{4\pi\epsilon_\circ}\frac{Z_P Z_T e^2}{2R_c}\left(3 - \frac{r^2}{R_c^2}\right), \; r < R_c \tag{3}$$

where R_c is the Coulomb radius, and Z_P and Z_T denote the charges of the projectile P and the target nuclei T, respectively. The centrifugal potential is

$$V_{\text{Centrifugal}}(r) = \frac{\hbar^2\, l\,(l+1)}{2\,\mu\, r^2} \tag{4}$$

where μ is the reduced mass of the colliding pair.

2.2. Nucleon-nucleon double folding model (NN-DFM)

In this study, the reaction observables are calculated by using the NN-DFM which uses the nuclear matter distributions for projectile and target nuclei together with an effective NN interaction potential [19, 20]. Thus, the DFM potential is written as

$$V_{DFM}(\vec{r}) = \int\int \rho_P(\vec{r}_1)\rho_T(\vec{r}_2)\nu_{nn}(|\vec{r} + \vec{r}_2 - \vec{r}_1|)d\vec{r}_1 d\vec{r}_2. \tag{5}$$

The ν_{nn} is assumed as the Michigan 3 Yukawa effective interaction in the following form

$$\nu_{nn}(r) = 7999\frac{\exp(-4r)}{4r} - 2134\frac{\exp(-2.5r)}{2.5r} - 276(1 - 0.005E/A_p)\delta(r)(\text{MeV}). \tag{6}$$

In addition, the the imaginary part of the optical model potential is taken as the Woods-Saxon shape. Thus, the nuclear potential is given as

$$V_{\text{Nuclear}}(r) = V_{DF}(r)N_R + \frac{-W_0}{1 + \exp\left(\frac{r - r_w(A_P^{1/3} + A_T^{1/3})}{a_w}\right)}, \tag{7}$$

where N_R is renormalization factor, and W_0, r_w and a_w are the depth, radius, and diffuseness parameter of the imaginary potential.

2.3. Fusion cross-section

The fusion reaction is crucial for nucleosynthesis and burning reactions at astrophysical energies. It is also very important in understanding the dynamics and structure of the astrophysical reactions. Fusion cross-section is usually calculated using either an incoming wave boundary condition (IWBC) or an imaginary potential. In our study, we have obtained the fusion cross-section via FRESCO [21] based on the barrier penetration model (BPM). In the BPM, fusion cross-section is given by

$$\sigma(E) = \sum_{\ell=0}^{\infty} \sigma_{\ell}(E) = \frac{\pi}{k^2} \sum_{\ell=0}^{\infty} (2\ell + 1)\, T_{\ell}(E), \quad T_{\ell}(E) = (1 - |S_{\ell}|^2) \tag{8}$$

where $T_{\ell}(E)$ is the quantum-mechanical transmission probability through the potential barrier. $T_{\ell}(E)$ is obtained by numerical integration of the Schrödinger equation as follows

$$\frac{d^2 u_{\ell}(r)}{dr^2} + \frac{2\mu}{\hbar^2}[E - V_{\text{Effective}}(r)]\, u_{\ell}(r) = 0, \tag{9}$$

where μ is the reduced mass of the projectile and target. The code DFPOT [22] is used for the DFM potential calculations, and the code FRESCO [21] is applied to get all the reaction observables.

2.4. Astrophysical S-factor

The astrophysical S-factor is a very significant observable for astrophysical environments at low energies. The S-factor is a slowly varying function of the energy E for non-resonant structure and it helps us to find the value of $S(0)$ close to zero by extrapolation [23], is defined as follows:

$$S(E) = \sigma(E) E exp(2\pi\eta) \tag{10}$$

This $S(E)$ equation shows a strong energy dependence, and η is given as the Sommerfeld parameter

$$\eta = \frac{Z_1 Z_2 e^2}{\hbar} \sqrt{\frac{\mu}{2E}}. \tag{11}$$

2.5. Density distributions of ^{12,13}C nuclei

In this section, we introduce five different density distributions of the ^{12,13}C nuclei which is used to make a comprehensive analysis for the ^{13}C + ^{12,13}C reaction observables.

2.5.1. Relativistic mean field (RMF)

The first density distribution of the ^{12,13}C projectile is assumed as the RMF density distribution that is reported by [24].

2.5.2. Gupta-1

The Gupta-1 density [25, 26] is taken as

$$\rho_i(r) = \frac{\rho_{0i}}{1 + \exp\left(\frac{r - R_{0i}}{a_i}\right)}, \quad \rho_{0i} = \frac{3A_i}{4\pi R_{0i}^3}\left(1 + \frac{\pi^2 a_i^2}{R_{0i}^2}\right)^{-1}, \tag{12}$$

where

$$R_{0i} = 0.90106 + 0.109\,57A_i - 0.0013A_i^2 + 7.714\,58 \times 10^{-6}A_i^3 - 1.621\,64 \times 10^{-8}A_i^4, \tag{13}$$

$$a_i = 0.34175 + 0.01234A_i - 2.1864 \times 10^{-4}A_i^2 + 1.46388 \times 10^{-6}A_i^3 - 3.24263 \times 10^{-9}A_i^4. \tag{14}$$

2.5.3. Gupta-2

The Gupta-2 density [27] based on equation (12) is assumed the following parameters

$$R_{0i} = 0.9543 + 0.0994A_i - 9.8851 \times 10^{-4}A_i^2 + 4.8399 \times 10^{-6}A_i^3 - 8.4366 \times 10^{-9}A_i^4, \tag{15}$$

$$a_i = 0.3719 + 0.0086A_i - 1.1898 \times 10^{-4}A_i^2 + 6.1678 \times 10^{-7}A_i^3 - 1.0721 \times 10^{-9}A_i^4. \tag{16}$$

2.5.4. NGO

The NGO density [28, 29] can be given as

$$\rho_{n(p)}(r) = \frac{\frac{3}{4\pi}\frac{N(Z)}{A}\frac{1}{r_{0n(0p)}^3}}{1 + \exp\left(\frac{r - C}{0.55}\right)}, \tag{17}$$

$$C = R\left(1 - \frac{1}{R^2}\right), \; R = \frac{N r_{0n} A^{1/3} + Z r_{0p} A^{1/3}}{A},$$
$$r_{0n} = 1.1375 + 1.875 \times 10^{-4}A, \; r_{0p} = 1.128 \text{ fm}. \tag{18}$$

where C is the central radius and Z, N and A are proton, neutron and mass numbers, respectively.

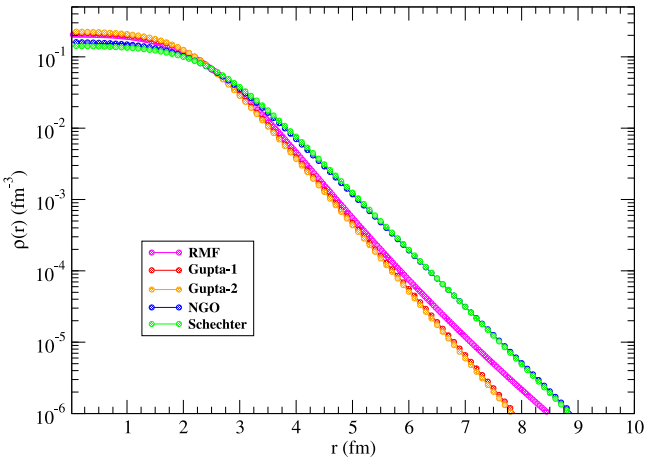

Figure 1. The changes with the distance (r) of RMF, Gupta-1, Gupta-2, NGO and Schechter densities of the ^{13}C nucleus.

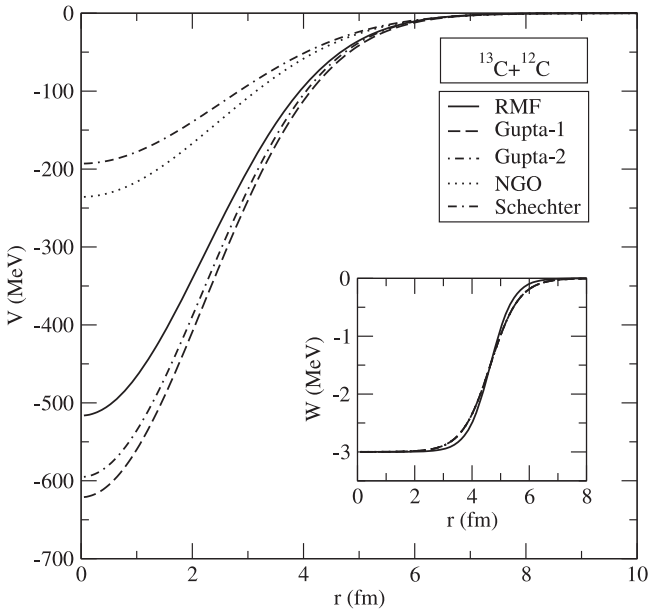

Figure 2. The real and imaginary potentials of $^{13}C + ^{12}C$ reaction by using given densities.

2.5.5. Schechter

The Schechter density [30] which has the same form with equation (12) can be written as

$$\rho_0 = \frac{0.212}{1 + 2.66A^{-2/3}}, \quad R_0 = 1.04A^{1/3}, \quad a = 0.54 \text{ fm}. \tag{19}$$

3. Results and discussions

3.1. $^{13}C + ^{12}C$ system

We have first calculated the fusion cross-section of the $^{13}C + ^{12}C$ system at energies near and below Coulomb barrier by using the RMF, Gupta-1, Gupta-2, NGO and Schechter densities of the ^{12}C and ^{13}C nuclei. The densities of ^{13}C which we used in this study are shown in figure 1.

We have presented that the real and imaginary potentials in figure 2. Additionally, the values of potential parameters used for the real and imaginary parts of the nuclear potential are shown in table 1. The χ^2 values are also given in table 1 in comparison with our density distributions results. We have presented the theoretical results together with experimental data in figure 3. Our analysis based on χ^2 calculations shows that the Gupta-1 density is significantly better than the others, and is in very good agreement with the experimental data.

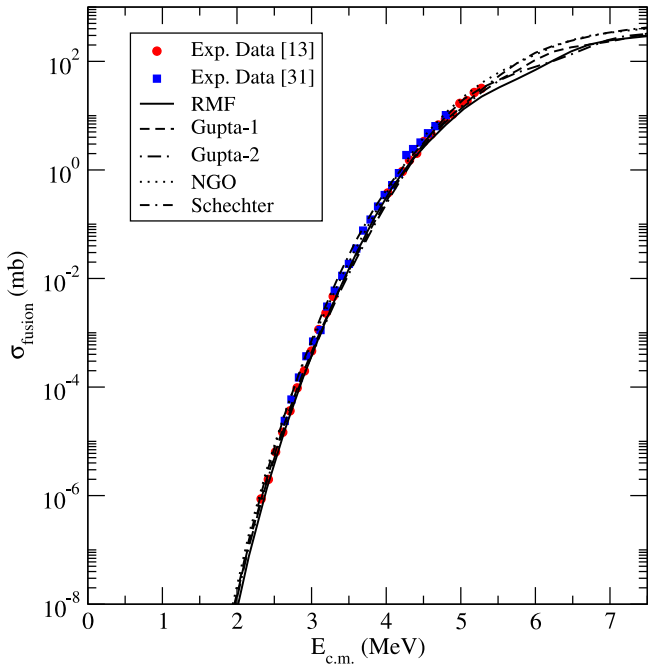

Figure 3. The fusion cross-sections of $^{13}C + ^{12}C$ reaction for five different densities as compared with the experimental data [13, 31].

Table 1. The optical potential parameters and χ^2 values of $^{13}C + ^{12}C$ fusion reaction for five different density distributions of carbon isotopes.

Reaction	Density	N_R	W(MeV)	r_w(fm)	a_w(fm)	χ^2
$^{13}C + ^{12}C$	RMF	1.27	3.0	1.0	0.40	14.93
	Gupta-1	1.50	3.0	1.0	0.50	4.59
	Gupta-2	1.40	3.0	1.0	0.50	9.63
	NGO	0.78	3.0	1.0	0.50	31.48
	Schechter	0.68	3.0	1.0	0.50	18.83

Then, we have calculated the S-factors of the $^{13}C + ^{12}C$ reaction for five different densities by using equation (10), and have compared our results together with different experimental data in figure 4. In this context, the RMF result produces the behavior of the data with correct phases and magnitudes at low energies until $E_{cm} = 4.5$ MeV although differences between RMF results and experimental data appear at forward energies. The Gupta-1 and Gupta-2 densities have given much more reasonable explanation compared to the RMF results at energies bigger than $E_{cm} = 4.5$ MeV.

Finally, we have presented the elastic scattering cross-sections of the $^{13}C + ^{12}C$ reaction for five different densities in figure 5 in order to make a comprehensive analysis. In this work, we have tried to use the same parameters simultaneously in order to reliably describe the observables of fusion cross-section, S-factor and elastic cross-sections. Therefore, we have changed the normalisation constant in only a few calculations in order to obtain the best fit with the experimental data. The reasonable results have been achieved with the data. We think that the main difference between experimental data and theoretical results is due to the different energy ranges of experimental data for fusion cross-section and elastic cross-sections.

In this study, we also investigated whether the Hindrance effect exists at low energies. In this effect, the S-factor reaches its maximum value at a certain energy at low energies and decreases sharply from this value, unlike the predictions of other models [11, 12]. In this study, as shown in the red circle in figure 6, we have not observed any Hindrance effect. Our results have showed a consistently increasing S-factor behaviour, obviously does not exhibit the sharp decline of the S-factor. This is in agreement with models in which the S-factor tends to increase towards low energies [7, 8, 10, 13].

3.2. $^{13}C + ^{13}C$ system

Here we have displayed the fusion cross-section of the $^{13}C + ^{13}C$ system calculated by using five different densities of the ^{13}C nucleus together with the experimental data in figure 7. The real and imaginary potentials for

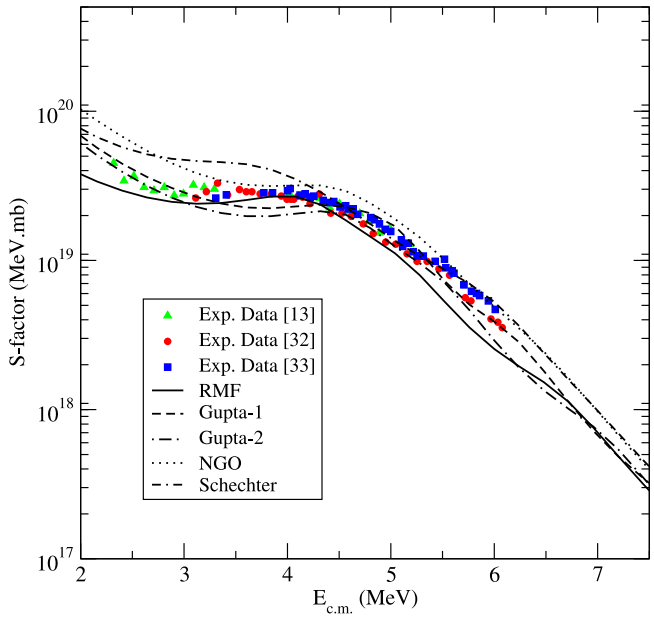

Figure 4. The results of $^{13}C + ^{12}C$ reaction S-factor for five different densities as compared with the experimental data [13, 32, 33].

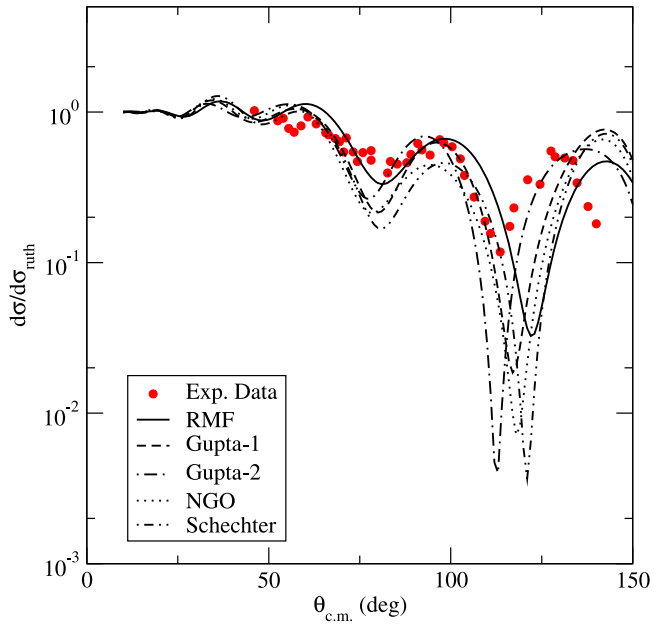

Figure 5. The elastic cross-sections of $^{13}C + ^{12}C$ reaction as compared with the experimental data at $E_{cm} = 7.8$ MeV [34].

the $^{13}C + ^{13}C$ system are shown in figure 8. Also, the parameters applied for the real and imaginary potentials and χ^2 values are listed in table 2. While the results display similar behavior at low energies, differences occur at higher energies. The RMF, Gupta-1 and Gupta-2 results show similarities with each other except for the NGO and Schechter results. According to the χ^2 values, the Gupta-2 density distribution has given better result than the other density distributions.

Then, we have given the S-factor results of $^{13}C + ^{13}C$ reaction in figure 9. We have compared the S-factor results with two different experimental results that we could obtain from the literature. As can be seen from figure 9, there are differences between the experimental results, especially at energies between $E_{cm} = 3$–4 MeV, which makes the theoretical analysis very difficult. The Gupta-1 and Gupta-2 results are similar and better than the results of other densities at low energies. However, the Gupta-1, Gupta-2 and RMF results show a similar behavior at higher energies although they show differences at medium energies. The NGO result captures slightly at low energies, but Schechter can not explain the experimental data in general. Based on these results, we

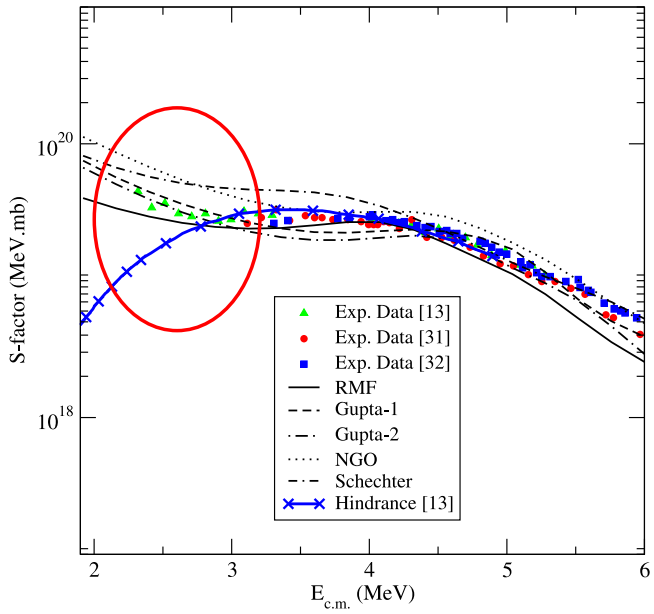

Figure 6. The comparison of our results and hindrance model results [13] for $^{13}C + ^{12}C$ reaction. The red circled region shows the difference between our results and the hindrance model.

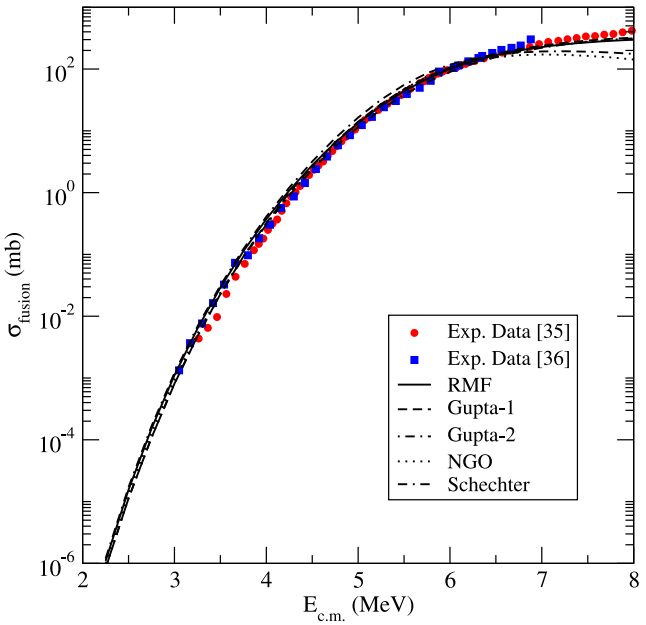

Figure 7. The fusion cross-sections of $^{13}C + ^{13}C$ reaction for five different densities of the ^{13}C nucleus as compared with the experimental data [35, 36].

can say that the Gupta-2 result may be an alternative density distribution for the analysis of the $^{13}C + ^{13}C$ reaction. Lastly, we have calculated the elastic cross-sections of the $^{13}C + ^{13}C$ reaction for the same density distributions and the same parameters used for fusion cross-section and S-factor observables. We have compared the theoretical results together with the data in figure 10. While the results of the densities generally explain the experimental data at low angles until $\theta = 60^0$, this harmony decreases at higher angles. In our calculations, we have used a weak short-range imaginary potential, which is localized at the Coulomb barrier. We have observed that the Gupta-1 density for the $^{13}C + ^{12}C$ reaction and the Gupta-2 density for the $^{13}C + ^{13}C$ reaction have given the best results compared to other densities. In this respect, we have examined the effect of imaginary diffusion parameter on the cross-sections of the $^{13}C + ^{12,13}C$ fusion reactions, and have shown the theoretical results for different imaginary diffusion parameters in figure 11. While the cross-sections are obtained, other potential parameters except the diffusion parameter have been kept constant. We have found

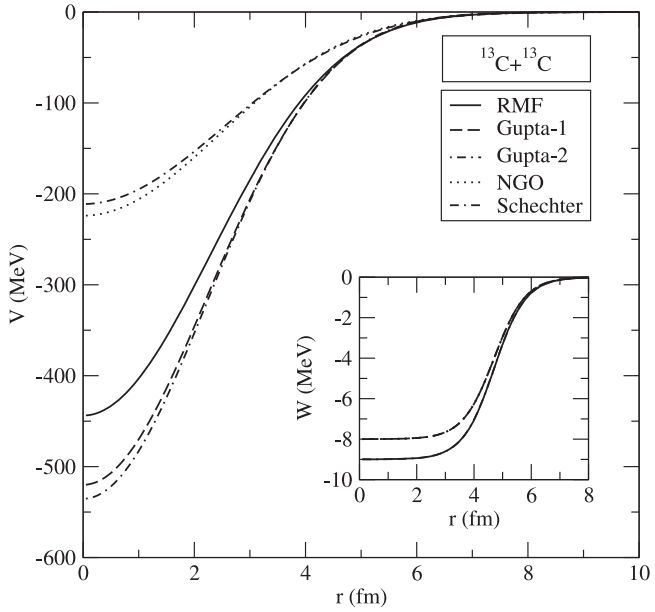

Figure 8. The real and imaginary potentials of $^{13}C + ^{13}C$ reaction for five different densities.

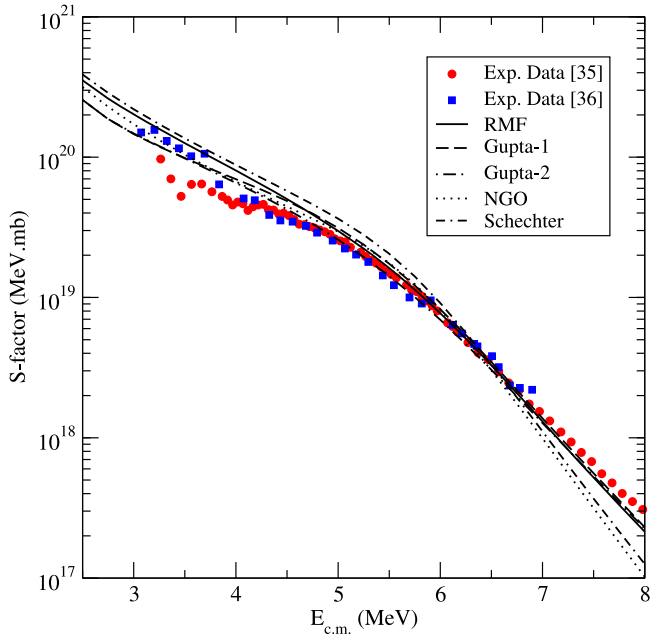

Figure 9. The S-factor results of $^{13}C + ^{13}C$ reaction for five different densities as compared with the experimental data [35, 36].

Table 2. The optical potential parameters and χ^2 values of $^{13}C + ^{13}C$ fusion reactions for five different density distributions of carbon isotopes

Reaction	Density	N_R	W(MeV)	r_w(fm)	a_w(fm)	χ^2
$^{13}C + ^{13}C$	RMF	1.12	9.0	1.0	0.55	6.10
	Gupta-1	1.20	8.0	1.0	0.55	4.70
	Gupta-2	1.20	8.0	1.0	0.55	2.41
	NGO	0.70	8.0	1.0	0.55	4.27
	Schechter	0.70	9.0	1.0	0.55	15.51

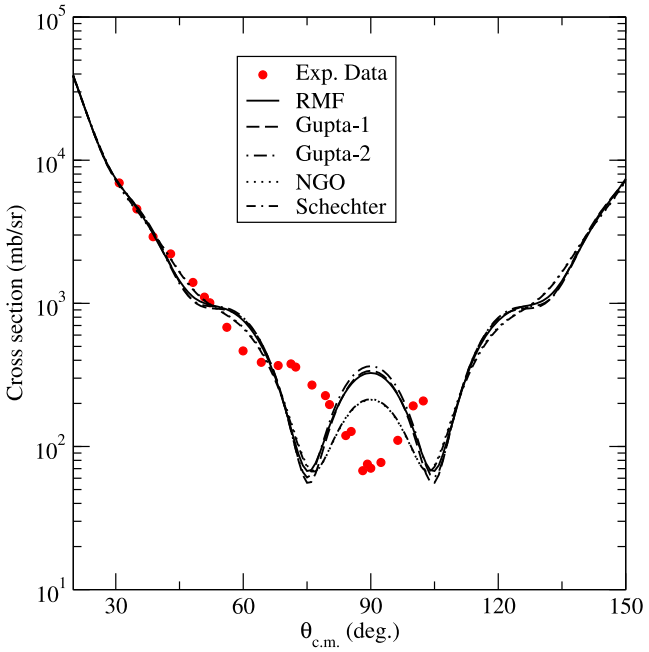

Figure 10. The elastic cross-sections of $^{13}C + ^{13}C$ reaction as compared with the experimental data at $E_{cm} = 7$ MeV. [35].

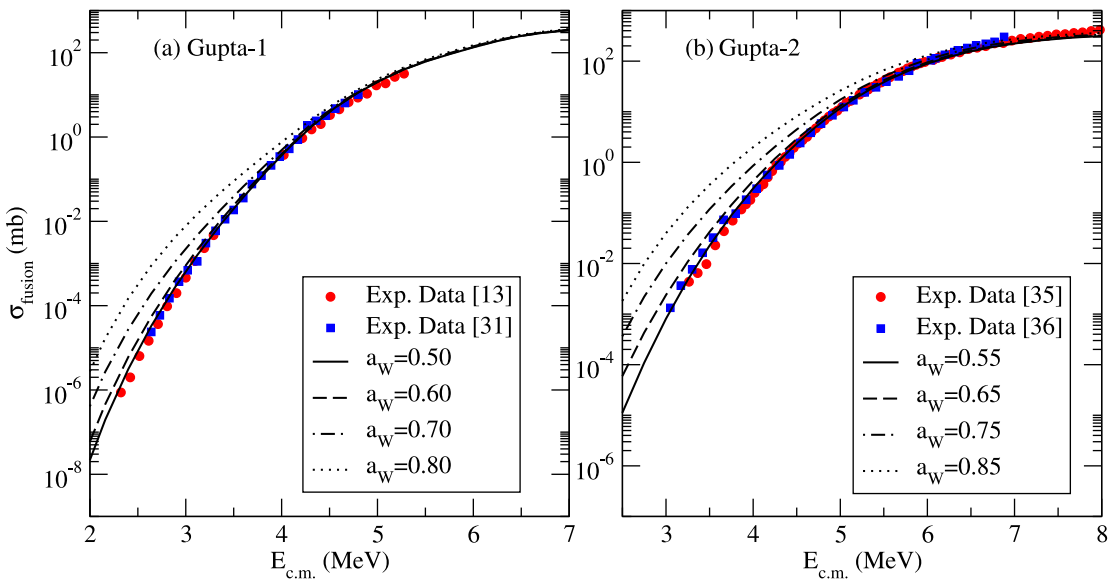

Figure 11. (a) The Gupta-1 result of the fusion cross-sections for the $^{13}C + ^{12}C$ reaction, (b) the Gupta-2 result of the fusion cross-sections for the $^{13}C + ^{13}C$ reaction obtained by using different imaginary diffusion parameters as compared with the experimental data [13, 31, 35, 36].

that the diffuseness parameter of imaginary potential has a significant effect on the fusion cross-section as expected [37]. It has been observed that the cross-sections for the results of both NGO and Gupta-2 densities have changed according to different diffusion parameters and could not explain the experimental data as the diffusion value increased.

4. Summary and conclusions

In this study, we have searched the relationship between structure and reaction observables for the $^{12,13}C + ^{13}C$ reactions. For this purpose, we have investigated the structure of the $^{12,13}C$ nuclei with five type density distributions. We have aimed to explain the fusion cross-sections, S-factor and elastic cross-sections observables for the $^{13}C + ^{12}C$ and $^{13}C + ^{13}C$ systems by using a realistic potential approach simultaneously.

Firstly, we have presented the $^{13}C + ^{12}C$ reaction theoretical results for the densities. The agreement between the theoretical results and the experimental data is excellent as shown in figure 3. It is clearly seen from figure 4, that the Gupta-1 and Gupta-2 results predict well the behaviour of S-factor for three different experimental data and produces the oscillatory structure data with correct phases and magnitudes. But, there are still some differences of magnitude between experimental data and theoretical results in different energy ranges. Then, we have examined the $^{13}C + ^{13}C$ system for the same observables. The Gupta-2 result gives best results for the fusion cross-sections as can be seen in figure 7. Additionally, our results show that the Gupta-2 result can be an alternative density distribution for the S-factor analysis of the $^{13}C + ^{13}C$ reaction. The elastic scattering results of the densities give an average behavior with the experimental data.

As a conclusion, we have obtained very good agreement between the experimental data and theoretical results, especially for the fusion cross-sections of the all reactions. Our results confirm the rising trend of S-factor as noted Zhang *et al.* [13] and references therein, and have given no evidence for the hindrance behavior. Finally, we have determined the importance of the diffusion parameter of the imaginary potential for the $^{12,13}C + ^{13}C$ fusion cross-sections. We have concluded that the structure of $^{12,13}C$ are very important to determine reaction observables at astrophysical energies, and should be considered very deeply for the reaction observables.

Data availability statement

All data that support the findings of this study are included within the article (and any supplementary files).

ORCID iDs

Murat Aygun https://orcid.org/0000-0002-4276-3511
Gokhan Kocak https://orcid.org/0000-0003-1784-7761

References

[1] Almqvist E, Bromley D A and Kuehner J A 1960 *Phys. Rev. Lett.* **4** 515–7
[2] Patterson J R, Winkler H and Zaidins C S 1969 *Astrophys. J.* **157** 367
[3] Gasques L R, Brown E F, Chieffi A, Jiang C L, Limongi M, Rolfs C, Wiescher M and Yakovlev D G 2007 *Phys. Rev. C* **76** 035802
[4] Spillane T *et al* 2007 *Phys. Rev. Lett.* **98** 122501
[5] Zhang N T *et al* 2016 *EPJ Web Conf.* **109** 09003
[6] Diaz-Torres A and Wiescher M 2018 *Phys. Rev. C* **97** 055802
[7] Umar A S, Uberacker V E and Horowitz C J 2012 *Phys. Rev. C* **85** 055801
[8] Aguilera E F *et al* 2006 *Phys. Rev. C* **73** 064601
[9] Esbensen H, Tang X and Jiang C L 2011 *Phys. Rev. C* **84** 064613
[10] Luo T P *et al* 2022 *Chin. Phys. C* **46** 064105
[11] Back B B, Esbensen H, Jiang C L and Rehm K E 2014 *Rev. Mod. Phys.* **86** 317
[12] Jiang C L, Rehm K E, Back B B and Janssens R V F 2007 *Phys. Rev. C* **75** 015803
[13] Zhang N T *et al* 2020 *Phys. Lett. B* **801** 135170
[14] Kocak G and Aygun M 2020 *Nucl. Phys. A* **1003** 122015
[15] Kocak G and Aygun M 2022 *Nucl. Phys. A* **1027** 122509
[16] Aygun M 2017 *Pramana Journal of Physics* **88** 53
[17] Aygun M and Aygun Z 2017 *Nucl. Sci. Tech.* **28** 86
[18] Satchler G R 1983 *Direct Nuclear Reactions* (*Oxford University Press, Oxford*) and *Introduction to Nuclear Reactions* (*The Macmillan Press Ltd, London 1980*)
[19] Satchler G R and Love W G 1979 *Phys. Rep.* **55** 183–254
[20] Brandan M E and Satchler G R 1997 *Phys. Rep.* **285** 143–243
[21] Thompson I J 1988 *Comput. Phys. Rept.* **7** 167
[22] Cook J 1982 *Comput. Phys. Commun.* **25** 125
[23] Burbidge M E, Burbidge G R, Fowler W A and Hoyle F 1957 *Rev. Mod. Phys.* **29** 547–650
[24] Kaki K 2017 *Prog. Theor. Exp. Phys.* **96** 093D01
[25] Gupta R K, Singh D and Greiner W 2007 *Phys. Rev. C* **75** 024603
[26] Ghodsi O N and Torabi F 2015 *Phys. Rev. C* **92** 064612
[27] Gupta R K, Singh D, Kumar R and Greiner W 2009 *J. Phys. G: Nucl. Part. Phys.* **36** 075104
[28] Ngô C, Tamain B, Beiner M, Lombard R J, Mas D and Deubler H H 1975 *Nucl. Phys. A* **252** 237
[29] Ngô H and Ngô C 1980 *Nucl. Phys. A* **348** 140
[30] Schechter H and Canto L F 1979 *Nucl. Phys. A* **315** 470
[31] Notani M *et al* 2012 *Phys. Rev. C* **85** 014607
[32] Dayras R A, Stokstad R G, Switkowski Z E and Wieland R M 1976 *Nucl. Phys. A* **265** 153–88
[33] Dasmahapatra B, Čujec B and Lahlou F 1982 *Nucl. Phys. A* **384** 257–72
[34] Fröhlich H, Bischof N, Tiereth W, Voit H, von Oertzen W and Imanishi B 1984 *Nucl. Phys. A* **420** 124–40
[35] Trentalange S, Wu S C, Osborne J L and Barnes C A 1988 *Nucl. Phys. A* **483** 406–28
[36] Chatterjee M L, Potvin L and Čujec B 1980 *Nucl. Phys. A* **333** 273–84
[37] Kocak G, Karakoc M, Boztosun I and Balantekin A B 2010 *Phys. Rev. C* **81** 024615